論文 / 著書情報
Article / Book Information

Title	FEASIBILITY STUDY ON RC MOMENT-RESISTING FRAMES INFILLED WITH CLT PANELS
Authors	Yasushi Sanada, Sujan Pradhan, R. Yoon, H. Isoda, J. Sakuta, T. Ohta, N. Kikuchi, S. Takabatake
Citation	Proceedings of the 18th World Conference on Earthquake Engineering, , ,
Pub. date	2024, 6

18TH WORLD CONFERENCE ON EARTHQUAKE ENGINEERING
WCEE2024
MILAN

MILAN, ITALY
30TH JUNE - 5TH JULY 2024
www.wcee2024.it

FEASIBILITY STUDY ON RC MOMENT-RESISTING FRAMES INFILLED WITH CLT PANELS

Y. Sanada[1], S. Pradhan[2], R. Yoon[1], H. Isoda[3], J. Sakuta[4], T. Ohta[4], N. Kikuchi[5] & S. Takabatake[5]

[1] Osaka University, Suita, Japan, sanada@arch.eng.osaka-u.ac.jp

[2] Tokyo Institute of Technology, Yokohama, Japan

[3] Kyoto University, Uji, Japan

[4] Horie Engineering and Architectural Research Institute Co., Ltd., Tokyo, Japan

[5] Daiho Corporation, Tokyo, Japan

Abstract: *This study proposes an innovative composite seismic wall incorporating Cross Laminated Timber (CLT) infill panels into Reinforced Concrete (RC) moment-resisting frames. The seismic behavior and performance were investigated through laboratory tests and numerical analyses. Two series of static cyclic loading tests were performed using scaled specimens representing single story RC weak column-strong beam and strong column-weak beam moment-resisting frames. The experimental investigation revealed that the presence of CLT infill significantly increased the lateral resistance of RC frames regardless the frame yield mechanisms. Furthermore, the deformation capacity was also improved particularly for the weak column-strong beam frame. The above experimental performance was well simulated by numerical analyses with macro modeling, which also clarified the lateral force-resisting mechanisms for the CLT panel infilled RC frames. These findings verified the feasible application of CLT panel infill to RC frames to have beneficial effects on the seismic performance.*

1. Introduction

Action to reduce CO_2 emission is a common human challenge for preventing global warming and realizing sustainable society. Japanese government has pledged to reduce emissions by 46% by 2030 compared to those in 2013 and achieve net-zero emission by 2050, as recorded by Ministry of Foreign Affairs of Japan (2021). From such social background, Japanese government has enforced the act to promote use of wood in buildings for sustainable society in 2021 (Ministry of Agriculture, Forestry and Fisheries 2021). Recently, Cross-Laminated Timber (hereafter, CLT) is getting popular for building material to realize the above promotion in Japan.

The CLT is manufactured by laminating and bonding timber strips so that the fiber directions are perpendicular; thus, it can be applied to shear (seismic) panel by eliminating its strong directivity. The objective of the present study is to investigate the feasible application of CLT panel to seismic wall in reinforced concrete (RC) buildings. Applications of the CLT panel to seismic devices in steel buildings have been studied by several researchers such as Aloisio et al. (2021) and Fukumoto et al. (2021). In contrast, few attentions have been paid to its application to RC buildings; a few researches were performed focusing on the feasibility of CLT panel as seismic retrofit devices for existing RC buildings by Stazi et al. (2019) and Aloisio et al. (2022). Thus,

fundamental data are still insufficient to realize seismic design of RC buildings combined with CLT seismic panels.

Considering the above background, in the present study, experimental and numerical studies were performed to investigate the effects of CLT infill panels in the in-plane direction on the seismic performance of RC moment-resisting frames. Two series of static cyclic loading tests were conducted using scaled specimens representing single story RC weak column-strong beam and strong column-weak beam moment-resisting frames, respectively. Then, the experimental behavior/performance was numerically simulated by macro analysis models, clarifying the lateral force-resisting mechanisms for the CLT panel infilled RC frames.

2. Experimental program

2.1. Test specimens

Two types of 40% scaled model frames were designed representing RC moment-resisting frame buildings. Four single story weak column-strong beam specimens were prepared for the first series, while five single story strong column-weak beam specimens were used for the second series. Within the present paper, however, two of them without/with CLT infill panels are focused from each test series: BF_wc-sb/WF_wc-sb and BF_sc-wb/WF_sc-wb from the first and second series, respectively.

2.1.1. Weak column-strong beam specimens

The specifications of specimens BF_wc-sb and WF_wc-sb are summarized in Table 1 compared to those of a prototype building in Japan. Figure 1 shows the rebar arrangements of RC members which are common for both specimens. The test parameter was absence/presence of the CLT panels shown in Figure 2. The timber species, layer structure, and thickness of the CLT panel were Japanese cedar, 5 layers 7 ply, and 86 mm, respectively. Rebar anchors of Φ6 were installed between both CLT panels in WF-wc-sb, as shown in Figure 2, while no anchor was applied to the boundaries of the CLT infill and surrounding RC members. The properties of concrete, reinforcement, and CLT from the material tests are summarized in Tables 2 to 4, respectively.

2.1.2. Strong column-weak beam specimens

The specifications of specimens BF_sc-wb and WF_sc-wb are summarized in Table 5 compared to those of another prototype building in Japan. Figure 3 shows the rebar arrangements of RC members which are common for both specimens. The test parameter was common with the first series: absence/presence of the CLT panels, as shown in Figure 4. The timber species, layer structure, and thickness of the CLT panel were Japanese cedar, 5 layers 5 ply, and 60 mm, respectively. No anchor was applied to the perimeters of CLT, while the CLT panels were embedded 5 mm into the RC beams, as shown in Figure 4. The tested material properties of concrete, reinforcement, and CLT are summarized in Tables 6 to 8, respectively.

Table 1. Specifications of the specimens for the first series.

Parameters	Prototype		Specimens	
	Column	Beam	Column	Beam
$B \times D$ (mm)	550×600	400×800	220×240	190×320
Long. rebar	10-D22 (SD345)	6-D25 (SD345)	4-D13 (SD345)	4-D19+4-D16 (SD345)
p_t	0.47	0.47	0.48	1.60
Shear rein.	D13@100 (SD295)	D13@200 (SD295)	D6@60 (SD295)	D10@60 (MK785)
p_w	0.46	0.32	0.48	1.25
CLT ($W \times H \times t$)	7,110mm×2,850mm ×210mm (4 pieces)		1,200mm×1,200mm ×86mm (2 pieces)	
CLT layup	5-layer 7-ply		5-layer 7-ply	
CLT tree species	Japanese cedar		Japanese cedar	

B: Member width, D: Member depth, p_t: Tensile reinforcement ratio (%), p_w: Shear reinforcement ratio (%), W: Width, H: Height, t: Thickness of CLT.

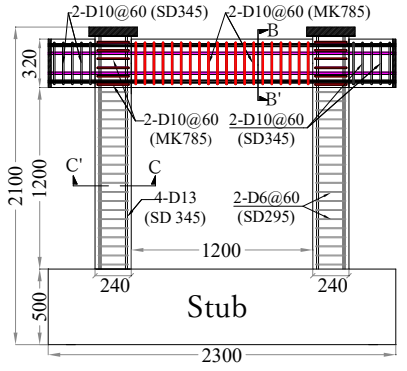

(a) Sectional elevation

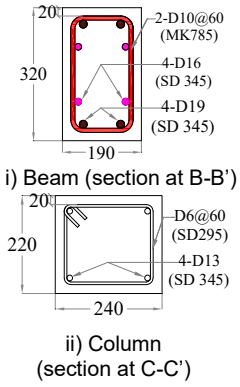

(b) Cross sections

Figure 1. Rebar details of RC members for the first series.

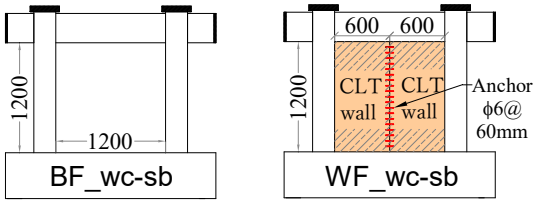

(a) BF_wc-sb (b) WF_wc-sb

Figure 2. Test parameter for the first series.

Table 2. Material properties of concrete for the first series.

Specimen	Elastic modulus	Compressive strength
BF_wc-sb	25×10^3 N/mm^2	30.5 N/mm^2
WF_wc-sb	24×10^3 N/mm^2	28.6 N/mm^2

Table 3. Material properties of reinforcement for the first series.

Rebar	Elastic modulus	Yield stress	Yield strain
D10 (SD345)	215×10^3 N/mm^2	420 N/mm^2	1.95×10^3 μ
D10 (MK785)	218×10^3 N/mm^2	851 N/mm^2	3.91×10^3 μ
D13 (SD345)	212×10^3 N/mm^2	401 N/mm^2	1.90×10^3 μ
D16 (SD345)	199×10^3 N/mm^2	380 N/mm^2	1.92×10^3 μ
D19 (SD345)	191×10^3 N/mm^2	388 N/mm^2	2.03×10^3 μ
D6 (SD295)	190×10^3 N/mm^2	430 N/mm^2	4.25×10^3 μ
Φ6 (SR295)	164×10^3 N/mm^2	337 N/mm^2	4.06×10^3 μ

Table 4. Material properties of CLT for the first series.

CLT type		Elastic modulus	Compressive strength
Full compression	Parallel to fiber on the surface	52×10^2 N/mm^2	22.0 N/mm^2
	Perpendicular to fiber on the surface	25×10^2 N/mm^2	9.14 N/mm^2
Partial compression	Parallel to fiber on the surface	47×10^2 N/mm^2	22.6 N/mm^2
	Perpendicular to fiber on the surface	24×10^2 N/mm^2	11.7 N/mm^2

Table 5. Specifications of the specimens for the second series.

Parameters	Prototype			Specimens		
	Column	Beam	Intermediate post	Column	Beam	Intermediate post
$B\times D$ (mm)	900×900	550×650	300×400	360×370	220×260	120×160
Long. rebar	14-D29 (SD390)	5-D25 4-D-25 (SD345)	8-D16 (SD295)	12-D13 (SD390)	10-D10 (SD345)	8-D10 (SD295)
p_t	0.32%	0.80% 0.64%	0.50%	0.29%	0.71%	0.74%
Shear rein.	D13@100 (SD295)	D13@100 (SD295)	D10@100 (SD295)	2-D6@60 (SD295)	4-D6@60 (SD295)	2-D4@50 (SD295)
p_w	0.28%	0.92%	0.48%	0.29%	0.96%	0.47%
CLT ($W\times H\times t$)	2850mm×2,310mm ×210mm (2 pieces)			1,110mm×870mm ×60mm (2 pieces)		
CLT layup	5-layer 7-ply			5-layer 5-ply		
CLT tree species	Japanese cedar			Japanese cedar		

B: Member width, D: Member depth, p_t: Tensile reinforcement ratio (%), p_w: Shear reinforcement ratio (%), W: Width, H: Height, t: Thickness of CLT.

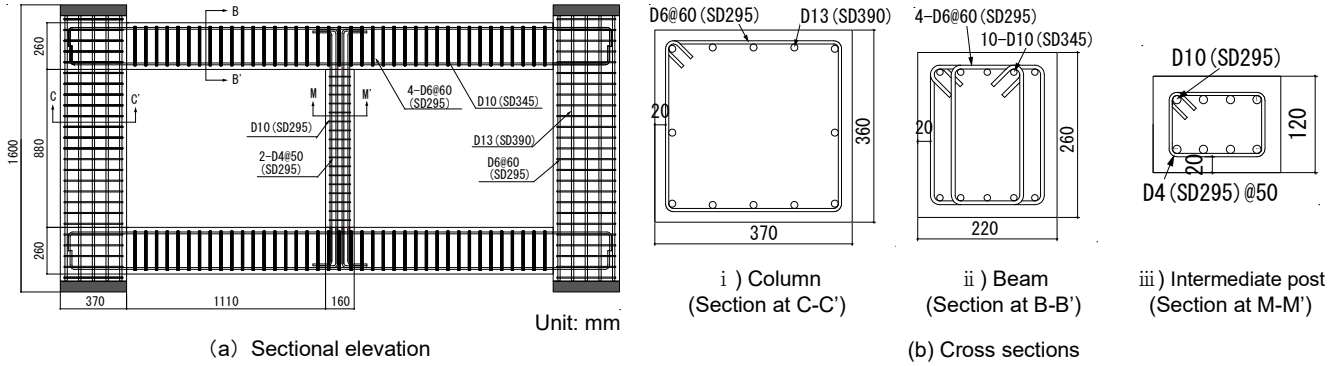

Figure 3. Rebar details of RC members for the second series.

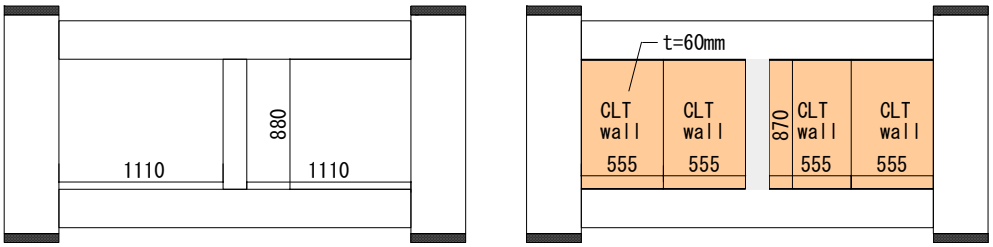

Figure 4. Test parameter for the second series.

Table 6. Material properties of concrete for the second series.

Specimen	Elastic modulus	Compressive strength
BF_sc-wb	26×10^3 N/mm^2	36.3 N/mm^2
WF_sc-wb	27×10^3 N/mm^2	37.8 N/mm^2

Table 7. Material properties of reinforcement for the second series.

Rebar	Elastic modulus	Yield stress	Yield strain
D4 (SD295)	199×10^3 N/mm^2	412 N/mm^2	4.07×10^3 μ
D6 (SD295)	189×10^3 N/mm^2	380 N/mm^2	4.06×10^3 μ
D10 (SD295)	183×10^3 N/mm^2	360 N/mm^2	1.96×10^3 μ
D10 (SD345)	180×10^3 N/mm^2	378 N/mm^2	4.11×10^3 μ
D13 (SD390)	182×10^3 N/mm^2	461 N/mm^2	2.54×10^3 μ

Table 8. Material properties of CLT for the second series.

CLT type		Elastic modulus	Compressive strength
Full compression	Parallel to fiber on the surface	74×10^2 N/mm^2	Full compression
	Perpendicular to fiber on the surface	64×10^2 N/mm^2	9.14 N/mm^2
Partial compression	Parallel to fiber on the surface	39×10^2 N/mm^2	Partial compression
	Perpendicular to fiber on the surface	32×10^2 N/mm^2	11.7 N/mm^2

2.2. Loading apparatus and protocols

The schematic views of the test apparatus for the first and second series are illustrated in Figures 5 and 6, respectively. The loading beam was fixed to the column tops of both specimens for the first series, while it was connected via pins up to a drift angle of 2.0% rad for WF_wc-sb, as shown in Figure 5, because of an underestimation of its lateral strength in design stage of the specimen. The effects of two different connection details on the specimen performance are discussed later with numerical analysis results. On the other hand,

in the second series, all column ends were connected to the foundation and loading beams via pins, as shown in Figure 6. A constant axial load equivalent to 15% of the column compressive strength was applied to all specimens for both series. Then, static cyclic loading was subjected to the specimens in the horizontal direction according to the loading histories shown in Figure 7. The horizontal loading was controlled by inter-story drift angles defined in Figures 5 and 6, respectively.

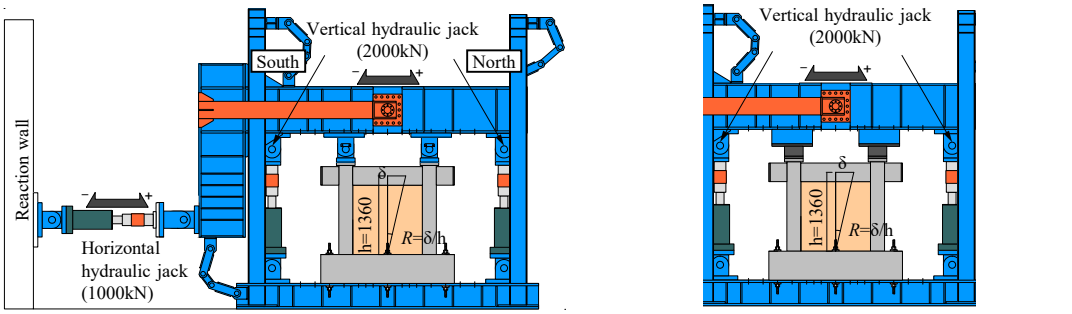

(a) WF_wc-sb (up to *R*=2.0% rad) (b) WF_wc-sb (beyond *R*=2.0% rad), BF_wc-sb

Figure 5. Test setup for the first series.

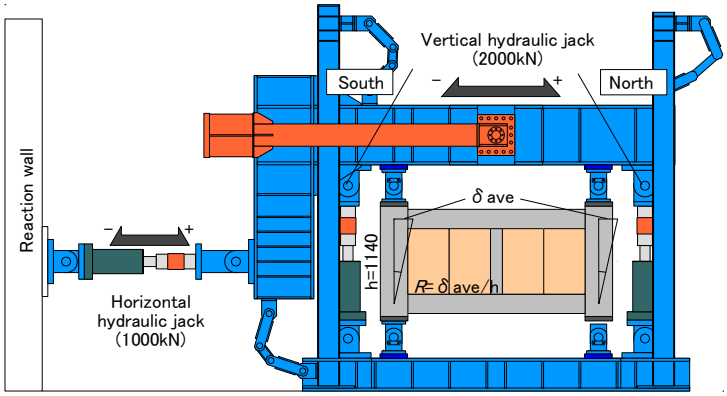

Figure 6. Test setup for the second series.

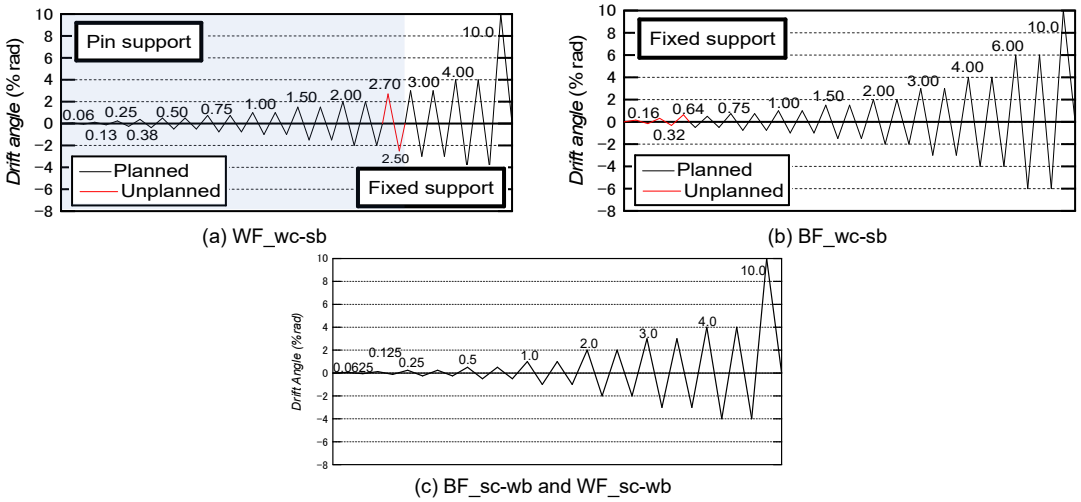

(a) WF_wc-sb (b) BF_wc-sb

(c) BF_sc-wb and WF_sc-wb

Figure 7. Loading histories in the horizontal direction.

3. Experimental results

The effects of the CLT infill on the seismic behavior/performance of the overall specimens were investigated through the hysteretic behavior under the cyclic lateral loading, damage progresses, and several indexes on the seismic performance.

3.1. Weak column-strong beam specimens

Figures 8 and 9 compare the lateral force vs. inter-story drift angle relationships and damage developments between BF_wc-sb and WF_wc-sb, respectively. The CLT infill panels began to independently rotate under the horizontal loading, as shown in Figure 10, which seemed that the panels pushed the upper/lower beam. Table 9 summarizes key indexes on the seismic performance such as initial stiffness, initial cracking, drift at

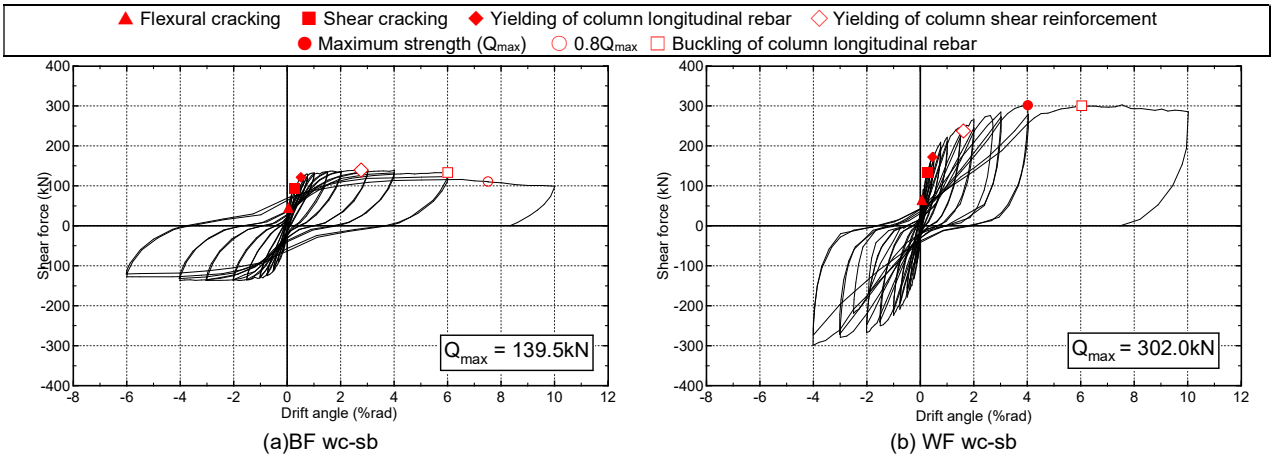

Figure 8. Lateral force vs. inter-story drift angle relationships of BF_wc-sb and WF_wc-sb.

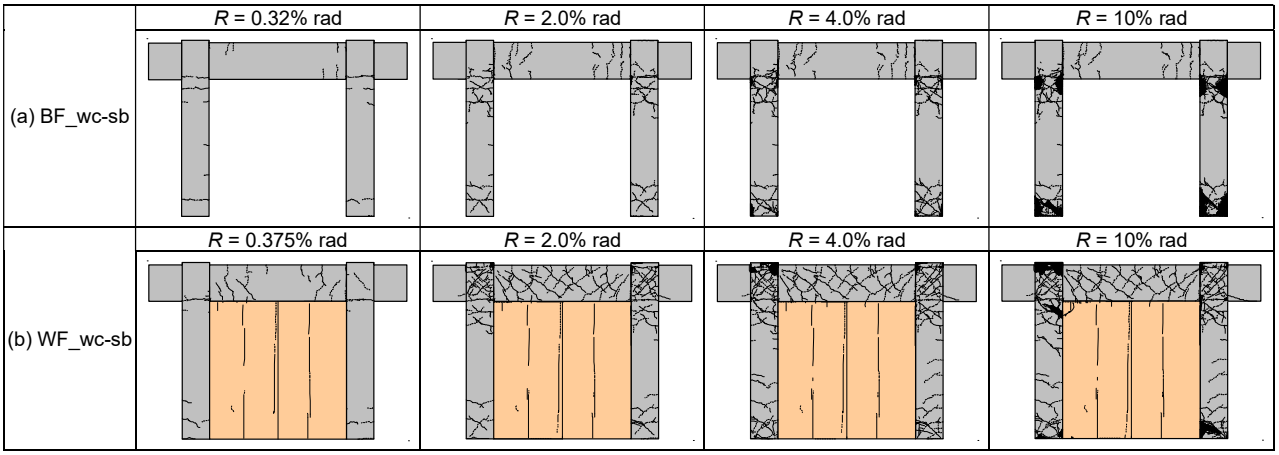

Figure 9. Damage developments of BF_wc-sb and WF_wc-sb.

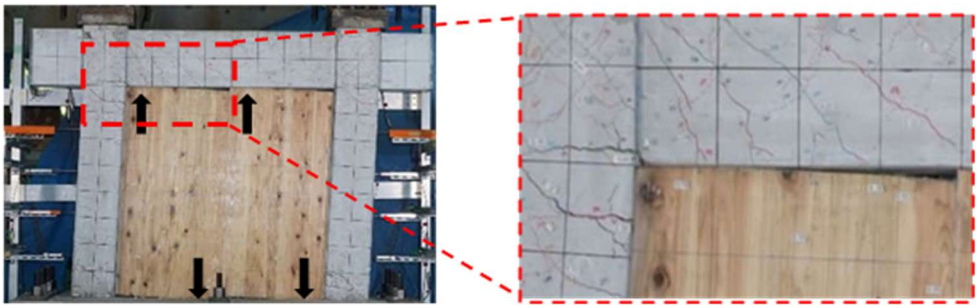

Figure 10. Typical rotational behavior of the CLT infill panels in WF_wc-sb.

yielding, and ultimate strength. Installing the CLT infill, the maximum strength of the specimen was increased more than twice, while the initial stiffness was increased approximately 10%. The shear forces at initial shear cracking on the RC columns were 92 kN and 161 kN for BF_wc-sb and WF_wc-sb, respectively, which were observed at drift angles of 0.3% rad to 0.4% rad, respectively. Initial yielding of the column longitudinal rebar was monitored at a little smaller drift angle in WF_wc-sb. The most remarkable behavior was the improvement of the column deformation capacity by installing the CLT infill; namely, the columns of WF_wc-sb approximately maintained their lateral resistance by a very high drift angle of 10% rad regardless of the plastic hinge formation at both ends.

Table 9. Comparisons on the seismic performance indexes between BF_wc-sb and WF_wc-sb.

Specimens	Initial stiffness	Initial shear cracking	Yielding of column long. rebar	Maximum strength
BF_wc-sb	68 kN/mm	92 kN at 0.32% rad	0.45% rad	139 kN at 3.0% rad
WF_wc-sb	72 kN/mm	161 kN at 0.38% rad	0.51% rad	302 kN at 4.0% rad

3.2. Strong column-weak beam specimens

The test results for the strong column-weak beam specimens are compared in Figures 11 and 12, and Table 10 in similar manners to Figures 8 and 9, and Table 9, respectively. In the case of the strong column-weak beam frame, the CLT infill significantly increased the initial stiffness as well as the maximum strength. The horizontal forces applied to the specimens at initial flexural cracking on the RC beams were approximately twice by the presence of infill. Initial yielding of the beam longitudinal rebar was observed at a smaller drift angle in WF_sc-wb. Similarly to the weak column-strong beam frame, no strength deterioration was observed by installing the CLT infill; in contrast, the lateral resistance of BF_sc-wb began to deteriorate beyond 2.0% rad drift angle.

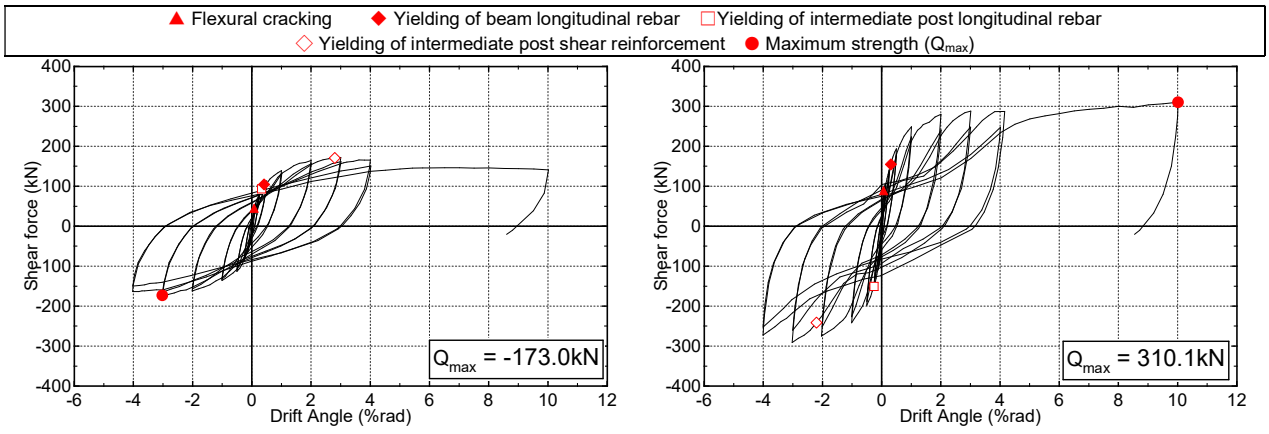

(a)BF sc-wb (b) WF sc-wb

Figure 11. Lateral force vs. inter-story drift angle relationships of BF_sc-wb and WF_sc-wb.

Table 10. Comparisons on the seismic performance indexes between BF_sc-wb and WF_sc-wb.

Specimens	Initial stiffness	Initial flexural cracking	Yielding of beam long. rebar	Maximum strength
BF_sc-wb	48 kN/mm	41 kN at 0.07% rad	0.41% rad	173 kN at 3.0% rad
WF_sc-wb	119 kN/mm	85 kN at 0.06% rad	0.31% rad	310 kN at 10.0% rad

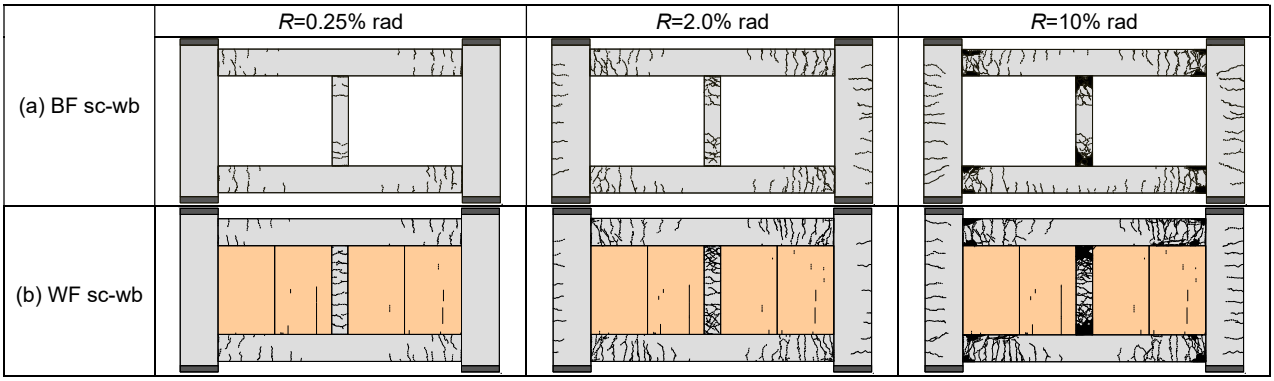

Figure 12. Damage developments of BF_sc-wb and WF_sc-wb.

4. Analytical modeling

Numerical analyses were performed using macro modeling to simulate the experimental behavior and performance of the specimens and to investigate a mechanism on the performance improvement by the CLT infill. Figure 13 illustrates the schematic views of the macro modeling for all specimens. In the case of WF_wc-sb, rotation at the RC column top was assumed to be free/fixed up to/beyond a drift angle of 2.0% rad considering the experimental setups, as illustrated in Figure 5. The RC columns and CLT infill panels were replaced by the multi-spring (MS) model by Li et al. (1988), in which the cross sections were replaced by concrete, steel, and CLT elements, as shown in Figure 14. The MS model was also used for the RC beams in the strong column-weak beam specimens, while those in the weak column-strong beam specimens were replaced by one component model with elastic/inelastic flexural springs and elastic axial and shear springs. Hognestad et al. (1955) model was applied to the CLT elements as well as concrete elements for the MS model, while an elastoplastic model was used for the steel elements, as shown in Figure 15. Parameters on the stress-strain model by Hognestad et al. were determined to simulate those from the material tests which are summarized on Tables 2 to 4 and 6 to 8; however, the values for CLT were from the partial compression tests on Tables 4 and 8. Figure 16 illustrates the inelastic characteristics for the one component model, in which structural parameters were evaluated according to Japanese design standards by Architectural Institute of Japan (2021).

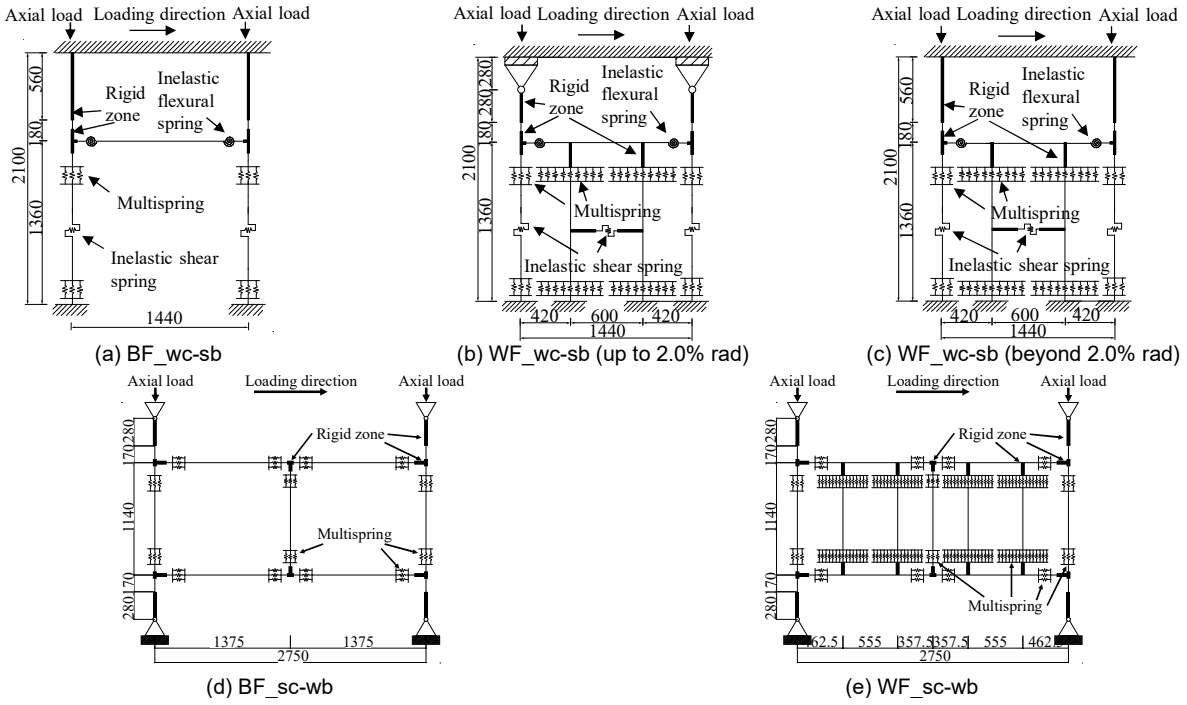

Figure 13. Overall modeling of all specimens.

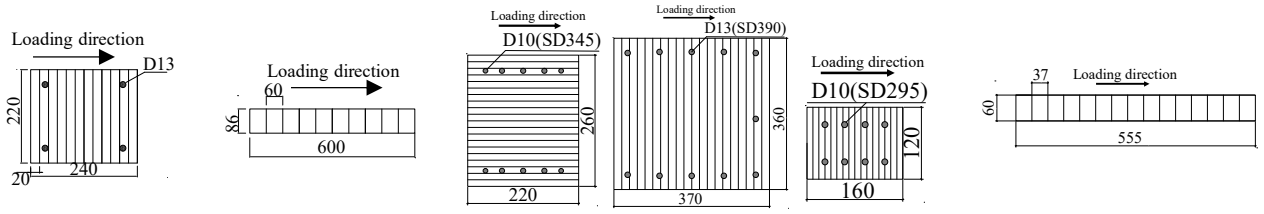

(a) Column in BF_wc-sb and WF_wc-sb

(b) CLT infill in WF_wc-sb

(c) Beam, column and intermediate post in BF_sc-wb and WF_sc-wb

(d) CLT infill in WF_sc-wb

Figure 14. Modeling of the cross sections of RC and CLT components.

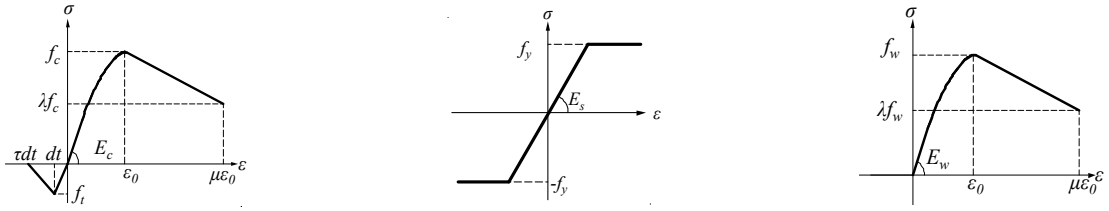

(a) Concrete model

(b) Steel model

(c) CLT model

Figure 15. Stress-strain behavior models for the MS model.

(a) Inelastic flexural spring model for beam in BF_wc-sb and WF_wc-sb

(b) Inelastic shear spring model for column in BF_wc-sb and WF_wc-sb

Figure 16. Inelastic behavior model for the one component model.

5. Numerical simulation results

Pushover analyses were performed for all specimens represented by the above numerical models. Figure 17 compares the performance curves evaluated by the analyses with the lateral force-drift angle relationships during the positive loading in the tests; however, the results were compared within 3.0% rad drift angle considering practical application.

5.1. Comparisons with the experimental results

The experimental envelop curves for both bare frame specimens: BF_wc-sb and BF_sc-wb were well simulated by the analyses regardless of different failure mechanisms of RC moment-resisting frames.

Focusing on the CLT infilled RC frame specimens, in the case of the weak column-strong beam specimen, WF_wc-sb, the performance curve also well agreed with the experimental envelop curve. In addition, comparing between two analytical results with/without a rotation freedom at the column top, it seemed that the change of connection details during the test did not significantly affect the seismic performance curves of the specimen.

On the other hand, in the case of the strong column-weak beam specimens, the performance curve beyond the flexural yielding showed a good agreement with the experimental envelop curve; however, the stiffness reaching the yielding was much lower in the analysis. This was likely to be caused by the neglection of the embedment of CLT infill into RC beams in the analysis, which might assume too lower tensile resistance on the cross section of CLT leading the stiffness degradation at an early stage.

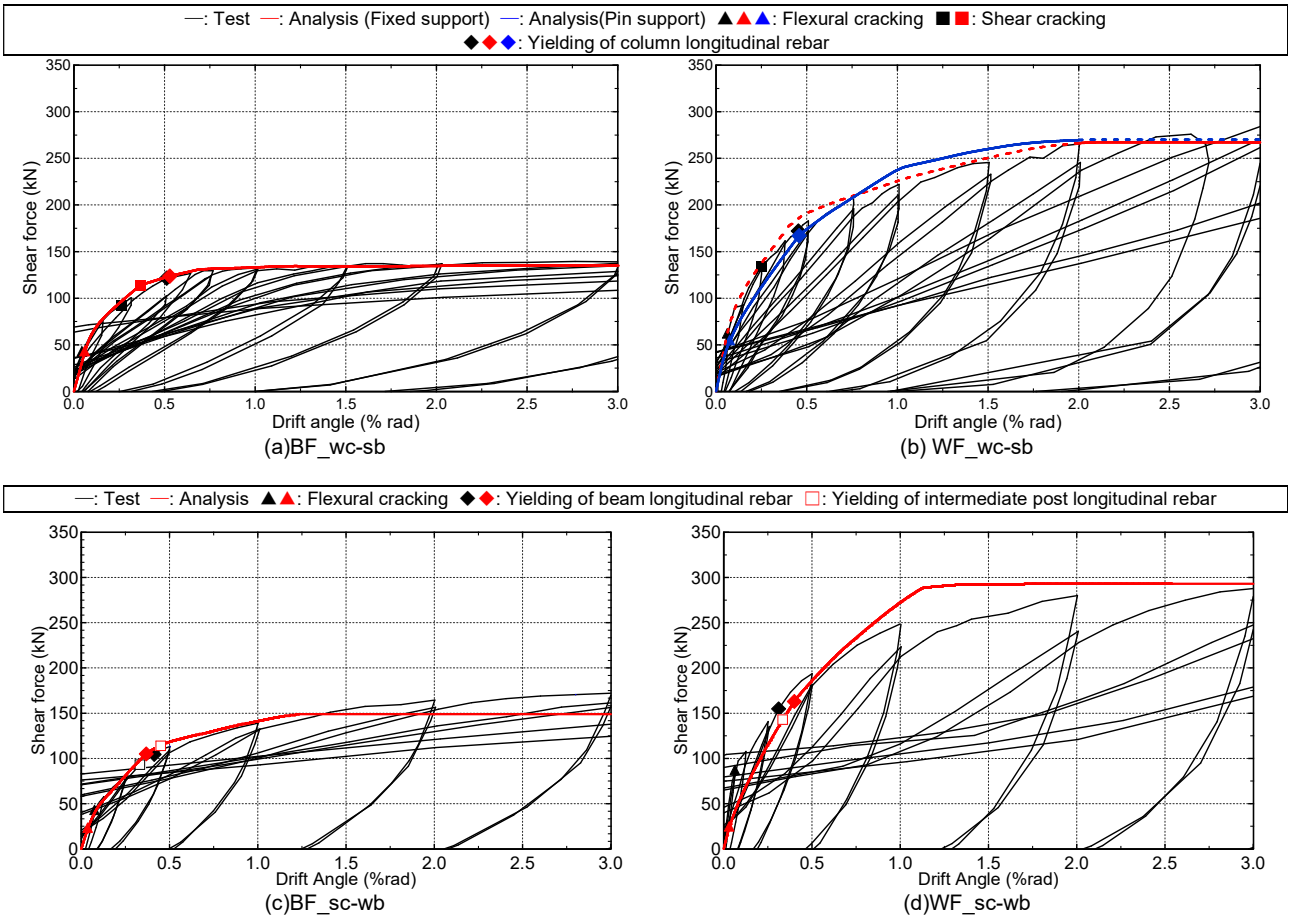

Figure 17. Comparisons between the analytical performance curve and experimental hysteretic behavior.

5.2. Discussions

Focusing on the weak column-strong beam specimen, WF_wc-sb, a mechanism resulting in the significantly high deformation capacity was investigated. Figure 18(a) shows the shear contributions of RC columns and CLT infill, respectively, in which the performance curve of BF_wc-sb without infill is also compared. The lateral resistance of BF_wc-sb, namely RC columns, became constant after yielding. In contrast, that of the RC columns in WF_wc-sb gradually decreased after yielding, while that of the CLT infill continuously increased. The mechanism behind such behavior is clarified by Figure 18(b) showing the axial contributions of RC columns and CLT infill in WF_wc-sb. It is found that the compressive forces initially supported by the RC columns shifted to the infill, which was likely to attribute to the rotational behavior of CLT panels, as illustrarted in Figure 10. Consequently, it was concluded that the RC columns could show higher ductility under lower axial loads according to the fundamental mechanics of RC structure.

On the other hand, in the case of the strong column-weak beam specimen, similar results of reduction of the column shear forces were observed by installing the CLT infill, as shown in Figure 19. Further study is necessary to clarify a mechanism showing high lateral resistance and ductility under hinging at the beam ends, while the performance curve was well simulated, as shown in Figure 17.

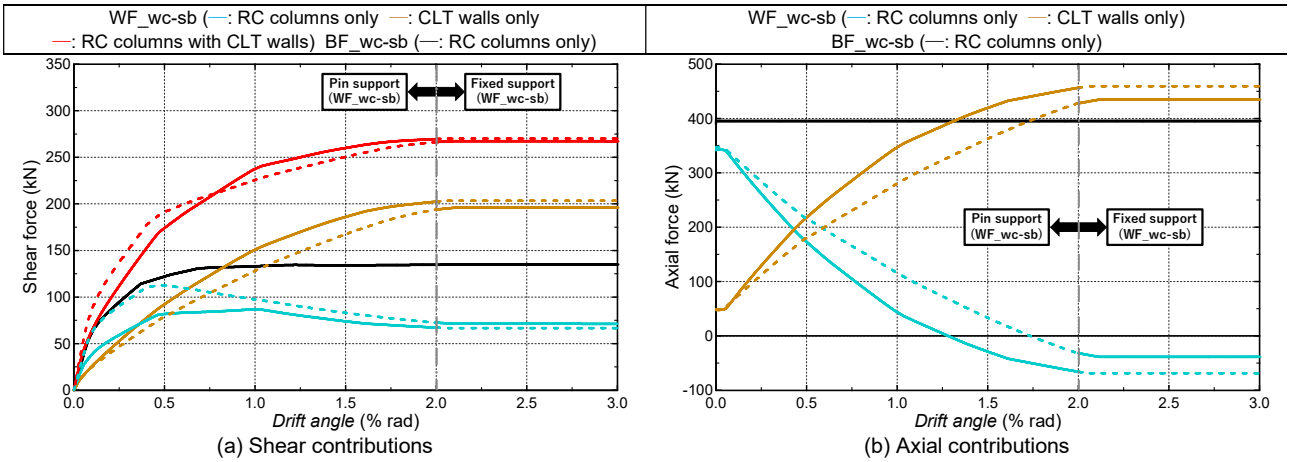

(a) Shear contributions (b) Axial contributions

Figure 18. Shear and axial contributions of the RC columns and CLT infill of WF_wc-sb.

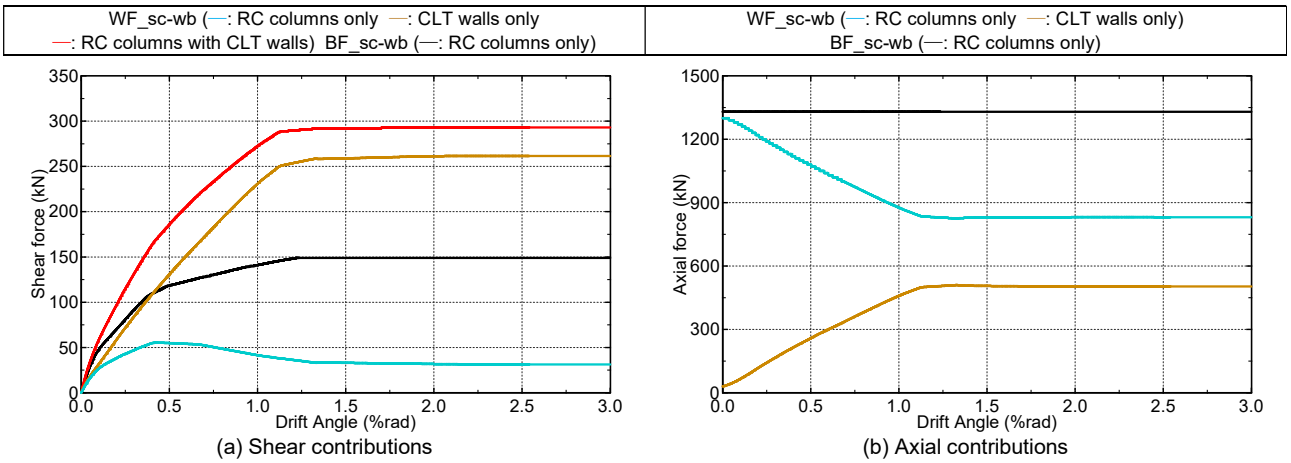

(a) Shear contributions (b) Axial contributions

Figure 19. Shear and axial contributions of the RC columns and CLT infill of WF_sc-wb.

6. Concluding remarks

An innovative composite seismic wall incorporating Cross Laminated Timber (CLT) infill panels into Reinforced Concrete (RC) moment-resisting frames was introduced and discussed through experimental and numerical studies. Major findings are summarized as follows:

The lateral resistance of RC moment-resisting frames was increased by installing the CLT infill.

The most remarkable finding was the improvement of the column deformation capacity by installing the CLT infill into the weak column-strong beam RC moment-resisting frame; namely, the columns of WF_wc-sb approximately maintained their lateral resistance by a very high drift angle of 10% rad regardless of the plastic hinge formation at both ends.

In the case of the strong column-weak beam frame, the CLT infilled RC frame specimen also showed excellent deformation capacity.

Numerical modeling presented in this study generally well simulated the performance curves of all specimens, indicating the feasibility of practical applications.

Based on the analytical results on the weak column-strong beam specimens with the CLT infill, a mechanism showing its very high deformation capacity was illustrated.

On the other hand, further study is needed to clarify a mechanism showing high lateral resistance and ductility for the strong column-weak beam frame.

7. Acknowledgements

The laboratory tests and numerical analyses were supported by Ms. Sugimoto K., Mr. Velazquez Mesa A., Mr. Murata A. and Mr. Nakashima H., graduate students at Graduate School of Engineering, Osaka University.

8. References

Aloisio A., Alaggio R., Fragiacomo M. (2021). Equivalent Viscous Damping of Cross-Laminated Timber Structural Archetypes, *Journal of Structural Engineering*, 147(4), https://doi.org/10.1061/(ASCE)ST.1943-541X.0002947.

Aloisio A., Boggian F., Tomasi R. (2022). Design of a novel seismic retrofitting system for RC structures based on asymmetric friction connections and CLT panels, *Engineering Structures*, 254(1), https://doi.org/10.1016/j.engstruct.2021.113807.

Architectural Institute of Japan. (2021). AIJ Standard for Lateral Load-carrying Capacity Calculation of Reinforced Concrete Structures (in Japanese).

Fukumoto K., Kouda M., Kubo K., Usami T., Kitamori A., Miyauchi Y., Isoda H. (2021) Experimental Study on CLT Seismic Panel Infilled within Steel Frame (in Japanese), *Journal of Structural and Construction Engineering*, Vol. 86, No. 787, pp. 1345-1356, https://doi.org/10.3130/aijs.86.1345.

Hognestad E., Hanson N.W., McHenry D. (1955). Concrete Stress Distribution in Ultimate Strength Design, *ACI Journal*, 52(12): 455-480.

Li K., Aoyama H., Otani S. (1988). Reinforced Concrete Columns under Varying Axial Load and Bi-Direction Lateral Load Reversal, *Proceedings of 9th WCEE*, Japan, pp. 537-544.

Ministry of Agriculture, Forestry and Fisheries (2021). https://www.rinya.maff.go.jp/j/riyou/koukyou/ (in Japanese).

Ministry of Foreign Affairs of Japan (2021). Prime Minister Suga's statement, https://www.mofa.go.jp/ic/ch/page6e_000236.html.

Stazi F., Serpilli M., Maracchini G., Pavone A. (2019). An experimental and numerical study on CLT panels used as infill shear walls for RC buildings retrofit, *Construction and Building Materials*, 211, 605-616, https://doi.org/10.1016/j.conbuildmat.2019.03.196.